Supplementary Materials

SUPPLEMENTARY METHODS

Lizard Tail Blastema Explant Culture

Lizard (*Anolis carolinensis*) tail blastemas were cultured as explants in a system previously used by our laboratory to culture CT explants (Lozito and Tuan, 2015). Lizard tails in the blastema stage of regeneration (10 days post tail loss by autotomy (10 DPA)) were obtained from reptile supply companies (Tails 'n More Pet Services and Underground Reptiles). Tails were swabbed with 70% isopropyl alcohol and soaked in Hank's Balanced Salt Solution (HBSS; Life Technologies) supplemented with 100 units/ml penicillin, 100 µg/ml streptomycin, and 250 ng/ml fungizone antimycotic (Life Technologies) for 30 min. Disinfected tails were trimmed 2 mm proximal to plane of original tail loss, which were easily identified by the abrupt transition from scaled original tail skin to unscaled blastema epidermis (Fig. S1A). When indicated, bead grafting or surgical manipulations (see below) were carried out at this point. Prepped blastemas were vertically positioned (original tail region oriented toward base of 96-well tissue culture plate) in chicken collagen type 1 (Col1) gels (EMD Millipore) and cultured at 30°C in lizard blastema explant medium (LBEM): 1:1 DMEM/Ham's F12 medium (Life Technologies) containing 50 µg/ml ascorbate (Sigma-Aldrich), 40 µg/ml L-proline (Sigma-Aldrich), 0.1 µM dexamethasone (Sigma-Aldrich), and 10 µg/ml insulin-transferrin-selenium (ITS) supplement (Life Technologies). When needed, LBEM was supplemented with various growth factors and/or drugs (see below). Liquid Medium height was adjusted during culture to maintain apical caps of blastema explants at liquid-air interfaces. Explants were cultured for 2 weeks, during which proximal and distal cartilage tube regions developed under control conditions (Fig. S1). At the conclusion of each experiment, tail tissue was extracted from collagen gel and processed for histology and immunostaining (see below). Cartilage formation and hypertrophy were compared between control and experimental conditions.

Lizard tail Blastema Cell Isolation and Culture

Lizard tail blastemas (10 days post tail loss by autotomy (10 DPA)) were collected and washed in HBSS supplemented with 100 units/ml penicillin, 100 µg/ml streptomycin, and 250 ng/ml fungizone antimycotic. Washed blastemas were incubated in 0.1% EDTA/HBSS for 45 min at room temperature with agitation, and epidermis was peeled from each blastema and discarded. Prepared blastemas were then washed extensively in HBSS, minced, and digested in 1 mg/ml trypsin (Sigma-Aldrich) and 1 mg/ml collagenase for 1 hour at 37°C. Blastema cells were collected in lizard blastema cell medium (LBCM) (DMEM/Ham's F12, 2 mM Glutamax, 0.1 µM dexamethasone, 40 µg/ml proline, 50 µg/ml ascorbate, and 10 µg/ml ITS supplement), seeded into V-bottom tissue culture plates (1 million cells per well), and pelleted by centrifugation at 500xg for 5 min. Blastema cell pellets were cultured at 30°C in LBCM for 3 weeks.

Lizard Periosteal Cell Isolation and Culture

Tail vertebrae were isolated from original lizard tails, spinal cords were removed, and vertebrae were trimmed to remove extreme proximal and distal ends. Prepped vertebrae consisted of relatively uniform, hollow vertebral tubes that facilitated

periosteum removal/isolation. Starting at the proximal end, periosteum was gently peeled from the underlying bone with fine-tipped forceps. Periosteum-free vertebrae were used in experiments testing the origins of the proximal CT. Periosteum pieces were collected and washed with HBSS before plating on tissue culture plastic in DMEM/Ham's F12 medium (Life Technologies) containing 10% fetal bovine serum, 100 units/mL penicillin, 100 µg/mL streptomycin, and 250 ng/mL Fungizone. Over one week of culture at 30°C, periosteal cells crawled out of periosteum pieces, creating "islands" around each piece, and cells were passaged once cell islands began to merge. Cells were collected and plated as micromass cultures according to previous reports (Mello and Tuan, 1999). Micromass cultures were analyzed for Alk Phos expression using the Leukocyte Alkaline Phosphatase Kit (Sigma) according to the manufacturer's instructions and immunostained for Col2.

Lizard Cartilage Callus (CC) and Cartilage Tube (CT) Cell Isolation

Regenerated lizard tails 10 weeks post autotomy and original tails were cut into sections approximately 1 cm in length, and tail sections were dissected with tungsten needles. Collected CCs and CTs were washed with HBSS, minced, and digested in 1 mg/ml trypsin and 1 mg/ml collagenase for 1 hour at 37°C to yield cell suspensions. CC/CT cells were plated on tissue culture plastic and expanded in DMEM/Ham's F12 supplemented with 10% fetal bovine serum, 100 units/mL penicillin, 100 µg/mL streptomycin, and 250 ng/mL Fungizone. Vertebral periosteal cells were isolated as described above. CC, CT, and vertebral cells were mixed 1:20 with unlabeled CC or CT cells and pellet cultured for 3 weeks. To identify CFDA-SE-labeled lizard cells, pellet sections were incubated with alkaline phosphatase-conjugate anti-FITC antibodies (Vector Labs), developed with Vector® Blue alkaline phosphatase substrate, and counterstained with methyl green.

Lizard Tissue-Chick Limb Bud Cell Xenogeneic Co-Cultures

Lizard vertebrae and CTs were isolated from original and regenerated lizard tails, respectively. Chick limb bud cells were isolated from Hamburger-Hamilton stage 23-24 embryonic limb buds digested in 1 mg/ml trypsin and 1 mg/ml collagenase and resuspended in Col1 gels at 20 million cells/ml (DeLise et al., 2000). Lizard vertebrae or CTs (5 mg wet weights) were placed in 96-well plates and covered with 100 µl chick cell/Col1 gel suspensions. Lizard tissue-chick limb bud cell co-cultures were maintained in 1:1 DMEM/F12, 1.1 mM $CaCl_2$, 1% glucose, 10% fetal bovine serum (FBS) (Life Technologies), 2.5 mM β-glycerophosphate, 0.3 mg/ml glutamine, 25 µg/ml ascorbate at 37°C. After 1 week, chick cells degraded and contracted Col1 gels around lizard tissues. After 21 days, co-cultures were collected and analyzed by collagen type X (Col10) immunostaining.

Migration Assays

Migration studies were performed using the Roche xCELLigence System (Limame et al., 2012; Lozito and Tuan, 2014). The system consists of modified Boyden chambers (CIM-Plate 16) with upper and lower chambers separated by a cell-permeable membrane lined with electrodes. Cells are seeded into the top chambers, and candidate chemoattractants are placed in the bottom chambers. As cells migrate across the membrane, they contact electrodes, which the system reads as migrating cells. Lizard CTs (5 mg wet weight), lizard vertebrae (5 mg wet weight), recombinant human BMP-2 (0-100

ng/ml), or negative controls were added to bottom wells, and Lizard periosteal cells (40,000 per well) were added to top wells. Serum-free LBEM was used in all experiments. Plates were scanned every 15 min for 24 hours.

Proliferation Assays

Adherent periosteal cell proliferation experiments were also performed using the xCELLigence System. Here, single-chambered "E-Plates" lined with electrodes were used to monitor cell numbers in real time. As cells proliferate, they contact electrodes, which the system reads as cell proliferation. The small surface area of the 96-well plate set-up combined with high electrode sensitivity makes this system particularly applicable for performing large numbers of replicates with small numbers of cells. Lizard periosteal cells were resuspended to 10000 cells/ml in serum-free LBEM supplemented with 0-100 ng/ml BMP-2, and 100 µl of cell suspensions were added to each well. Plates were scanned every 30 min for 100 hours.

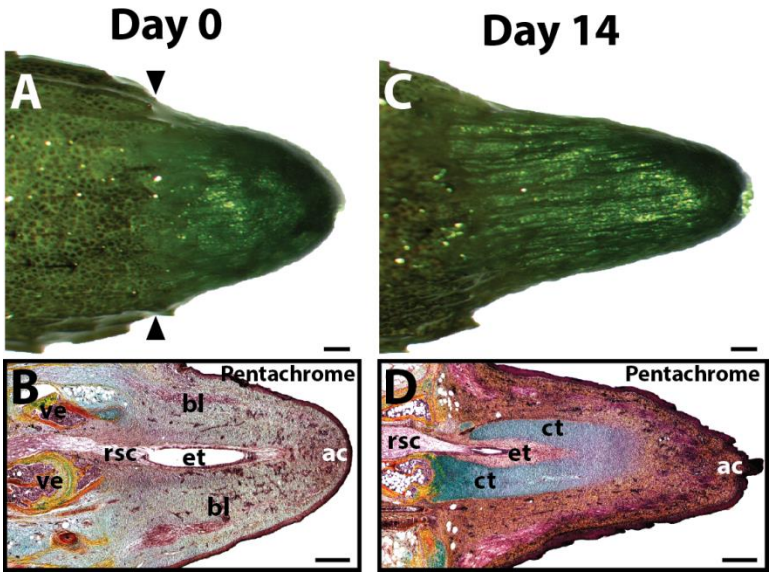

Fig. S1: Lizard tail blastema explant culture. (A) Gross morphology and **(B)** histological analysis (pentachrome) of representative lizard tail blastema isolated for explant culture (Day 0). Black arrow heads mark transition between original tail and blastema. **(C)** Gross morphology and **(D)** histological analysis (pentachrome) of representative lizard blastema at conclusion of explant culture (Day 14). ac, apical cap; bl, blastema; ct, cartilage tube; et, ependymal tube; rsc, regenerated spinal cord; ve, vertebra. Bar = 100 μm.

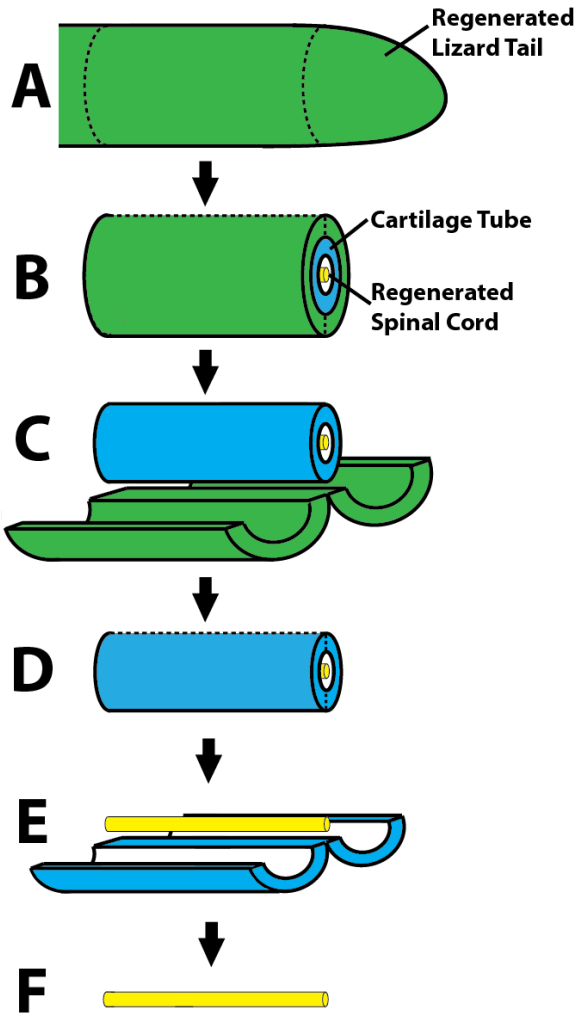

Fig. S2: Schematic of techniques used to isolate CTs and regenerated spinal cords. (A) Regenerated lizard tails (at least 60 DPA) were cut into 5 mm sections. **(B)** Tail sections were cut along the dorsal and ventral midlines down to the depth of the CT. **(C)** Skin, muscle, and connective tissue were laterally peeled to expose CTs. **(D)** In mature regenerates, there exists very little connection between CTs and non-skeletal tissues, and CTs are easily separated from other tail tissues. To isolate regenerated spinal cords, CTs were cut along the dorsal and ventral midlines to the depth of inner CT edge. **(E)** CTs were separated along cut lines. **(F)** Very few tissue connections exist between spinal cords and the CTs, and intact lengths of regenerated spinal cords are easily isolated from remaining CT tissue. Dashed lines denote cut lines.

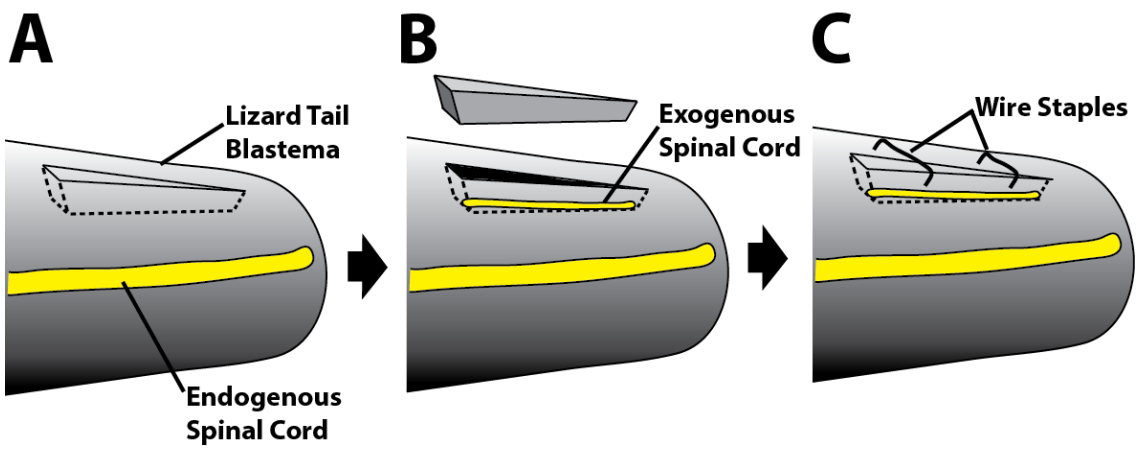

Fig. S3: Schematic of techniques used to transplant exogenous regenerated spinal cords into lizard blastemas. (A) Triangle-shaped incisions 1-2 mm in depth were made on the surfaces of lizard tail blastemas (9-12 DPA). **(B)** Wedge-shaped sections of blastemal tissue gently excised with watch forceps, creating V-bottomed troughs in the blastema. **(C)** Intact regenerated spinal cord pieces extracted from donor regenerated tails (see Fig. S2) were positioned along the bottoms of V-bottomed troughs. **(D)** Wedge-shaped blastemal tissues were replaced into troughs, on top of spinal cord pieces and **(E)** held in place with wire staples. Sham surgery (Control) involved identical steps except spinal cord pieces were omitted. Dashed lines denote cut lines.

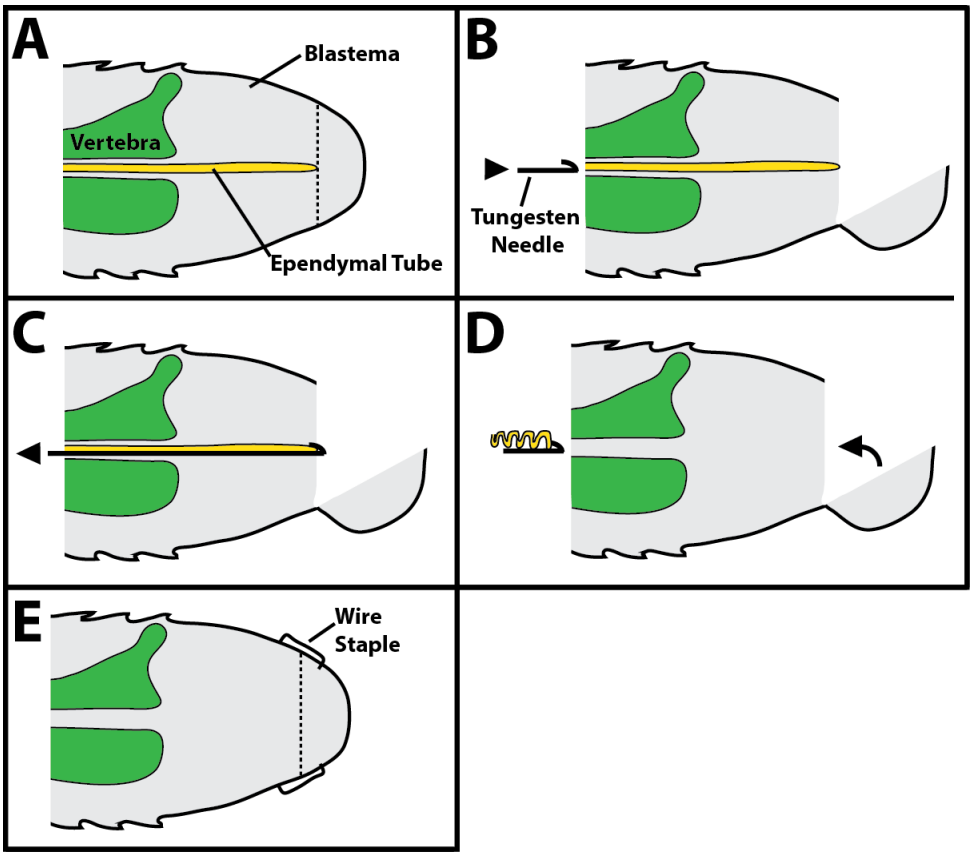

Fig. S4: Schematic of techniques used to remove ependymal tubes from lizard tail blastemas. (A) Lizard tail blastemas (9-12 DPA) with intact original tail vertebrae were cut 1-2 mm from the top. **(B)** Blastemal tips were separated along cut lines, and tungsten needles with tips modified into hooks were inserted into the spinal canals of original tail vertebrae. **(C)** Tungsten needles were guided along spinal canals into blastema tissue until just hooked tips emerged from cut planes. **(D)** The hooked tips were positioned along ependymal tubes, so that when needles were retracted, ependymal tubes were extracted. **(E)** Blastema tips were re-positioned and fixed into place with wire needles. Black arrow heads indicate motion of needles and tissue, and dashed lines denote cut lines.

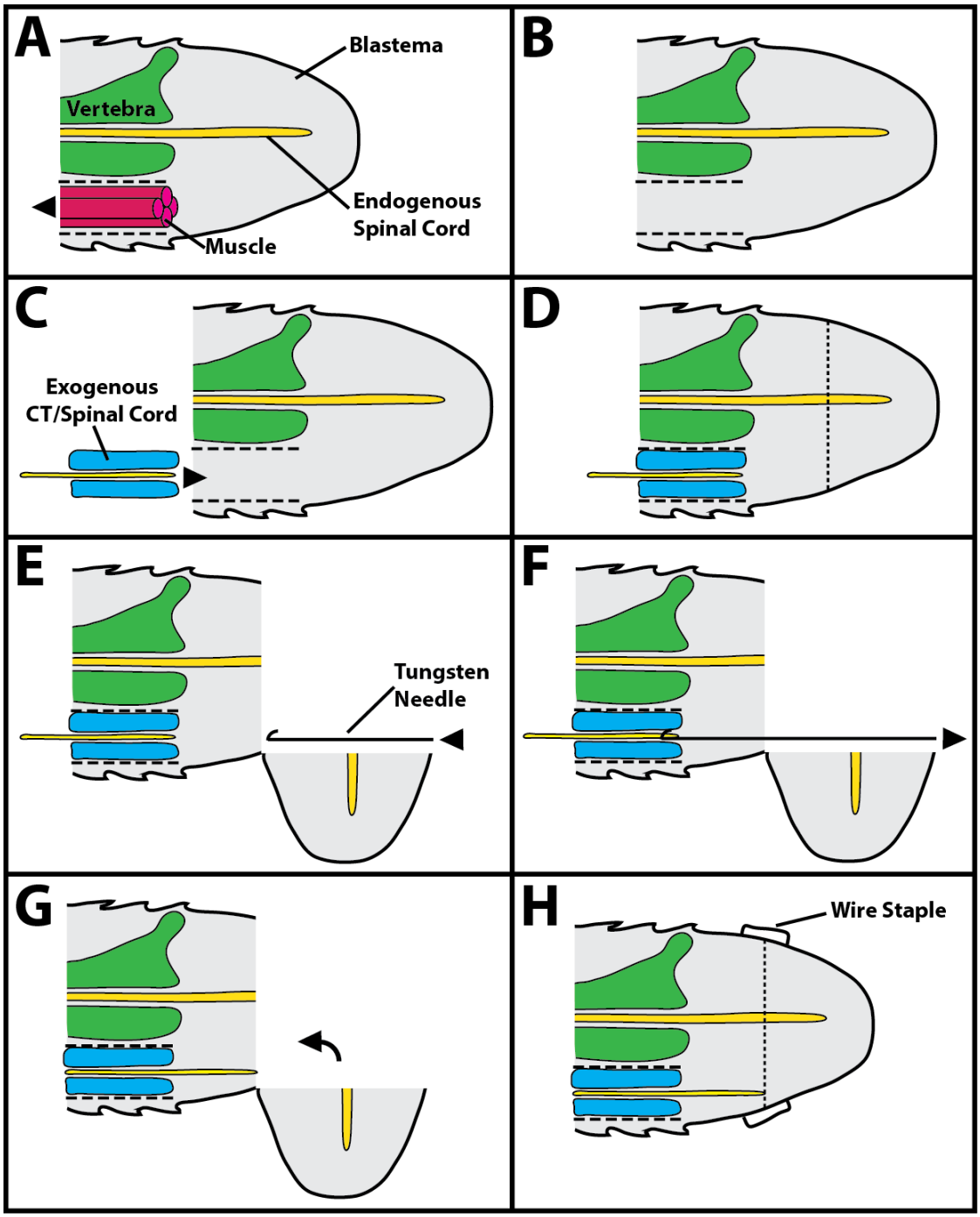

Fig. S5: Schematic of techniques used to relocate distal CTs into proximal tail regions. (A) Lizard blastemas (9-10 DPA) with intact original tail vertebrae were collected, and the connective tissue surrounding one of the ventral tail muscle bundles were cut. **(B)** Dorsal muscle bundle was removed and **(C)** replaced with exogenous CTs containing intact spinal cord isolated from donor regenerated lizard tails (see Fig. S2). **(D)** Blastemas were cut 1-2 mm from the tip. **(E)** Tip regions were separated from blastemas along cut lines. Tungsten needles with modified hooked tips were positioned in line with central canal of inserted CTs. **(F)** Needle tips were inserted into blastemas until hooked tips caught spinal cords of implanted CTs. Needles were retracted along original insertion paths, thereby extending exogenous spinal cords into blastema tissue. **(G)** Blastema tips were repositioned and **(H)** fixed in place with wire staples. Black arrow heads indicate motion of needles and tissue, and dashed lines denote cut lines.

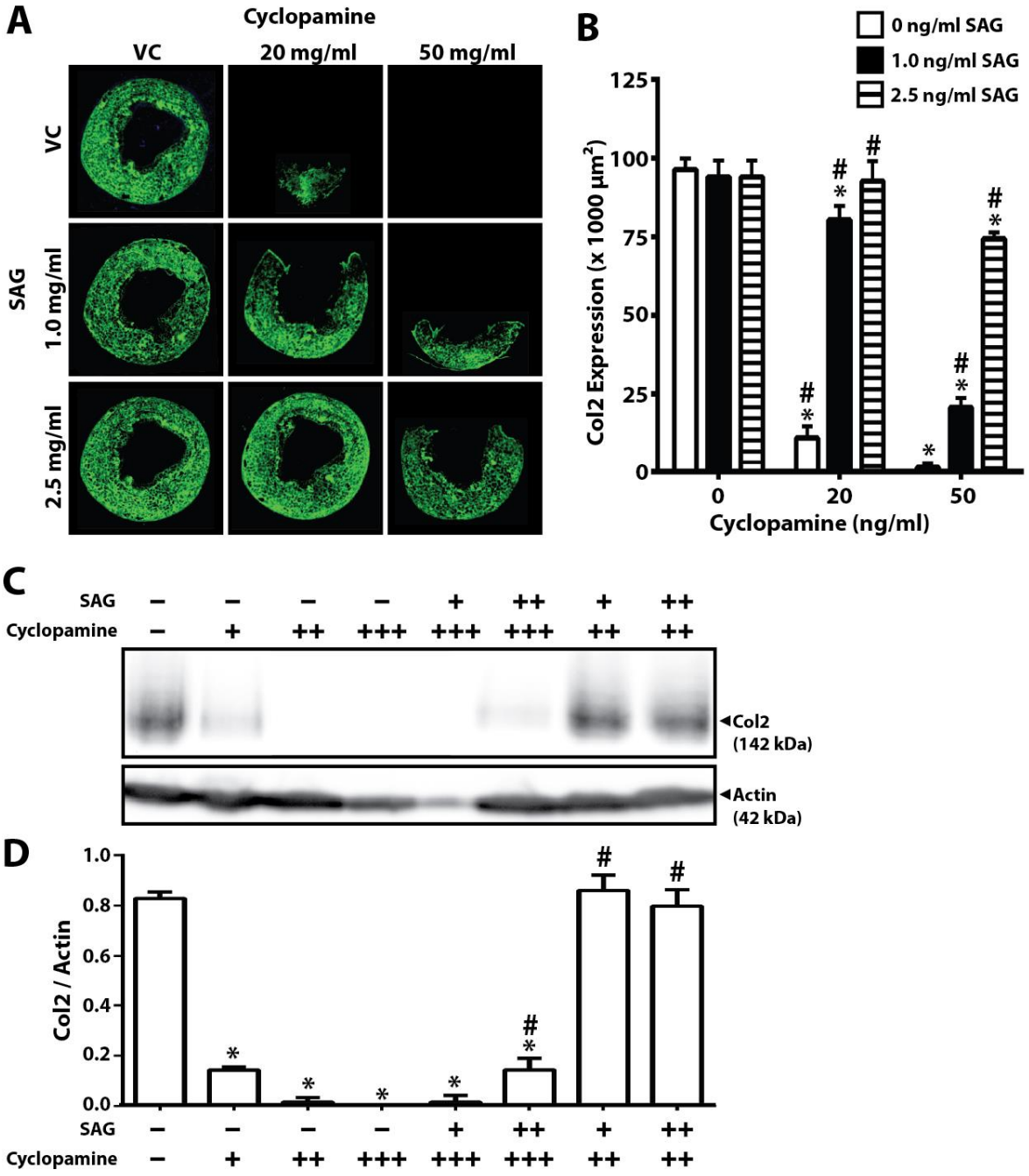

Fig. S6: Titration of cyclopamine and SAG concentrations for modulating lizard tail cartilage formation. (A, B) Titration of cyclopamine/SAG concentration combinations using drug-soaked beads. **(A)** Beads soaked in either vehicle control, cyclopamine (20 or 50 mg/ml), or SAG (2.5 or 1.0 mg/ ml) were implanted in the dorsal surfaces of lizard tail blastemas. These comparatively high drug loading concentrations were necessary due to the low release kinetics exhibited by the resin beads used and the impermeable nature of lizard tail tissues. Following 2 weeks of culture in vivo, blastemas were analyzed by Col2 immunofluorescence. **(B)** Col2 expression for each cyclopamine/SAG-soaked bead concentration combination was quantified as the area of fluorescent signal averaged over three technical replicates (n=3). *, $p < 0.05$ compared to 0 ng/ml cyclopamine condition; #, $p < 0.05$ compared to 0 ng/ml SAG condition. **(C, D)** Titration of cyclopamine/SAG concentration combinations using soluble drugs. **(C)** Lizard tail blastema explants were treated with 0 (-), 300 (+), 600 (++), or 900 (+++) nM cyclopamine and 0 (-), 40 (+), or 80 (++) nM and analyzed by Col2 and actin

Western blots. **(D)** Densitometric analysis of Col2/actin Western blots. Bands from Col2 blots were quantified using ImageJ and normalized to corresponding actin bands. Results are from three experimental replicates (n=3). *, $p < 0.05$ compared to 0 ng/ml cyclopamine condition; #, $p < 0.05$ compared to 0 ng/ml SAG condition.

For bead experiments, 20 mg/ml cyclopamine was sufficient for inhibiting dorsal Col2 expression **(A)**, and 2.5 mg/ml was effective at rescuing cyclopamine-inhibited Col2 expression **(A, B)**. For soluble drug experiments, 600 nM inhibited Col2 expression, while 40 nM SAG rescued Col2 expression **(C, D)**.

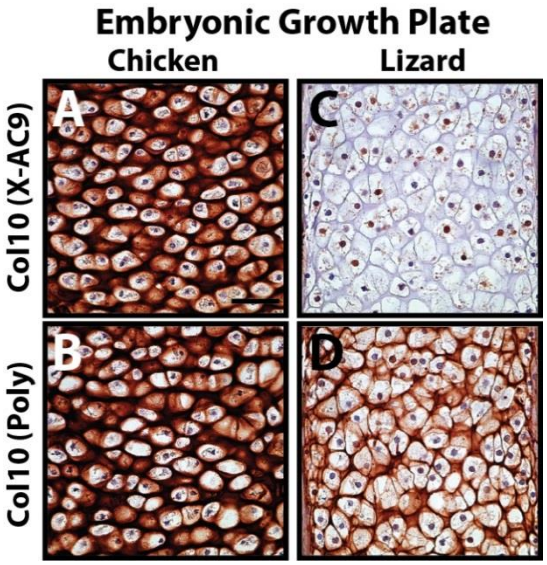

Fig. S7: X-AC9 antibody is specific for chicken, but not lizard, Col10. Growth plates of identically treated **(A, B)** day 11 chick legs and **(B, C)** day 20 embryonic lizard legs (femur) were immunostained using the **(A, C)** X-AC9 monoclonal Col10 antibody or **(B, D)** the polyclonal Col10 antibody (Poly; Abcam ab58632). The X-AC9 antibody reacted with chicken, but not lizard, Col10, while the polyclonal antibody recognized both lizard and chicken Col10. Bar = 50 μm.

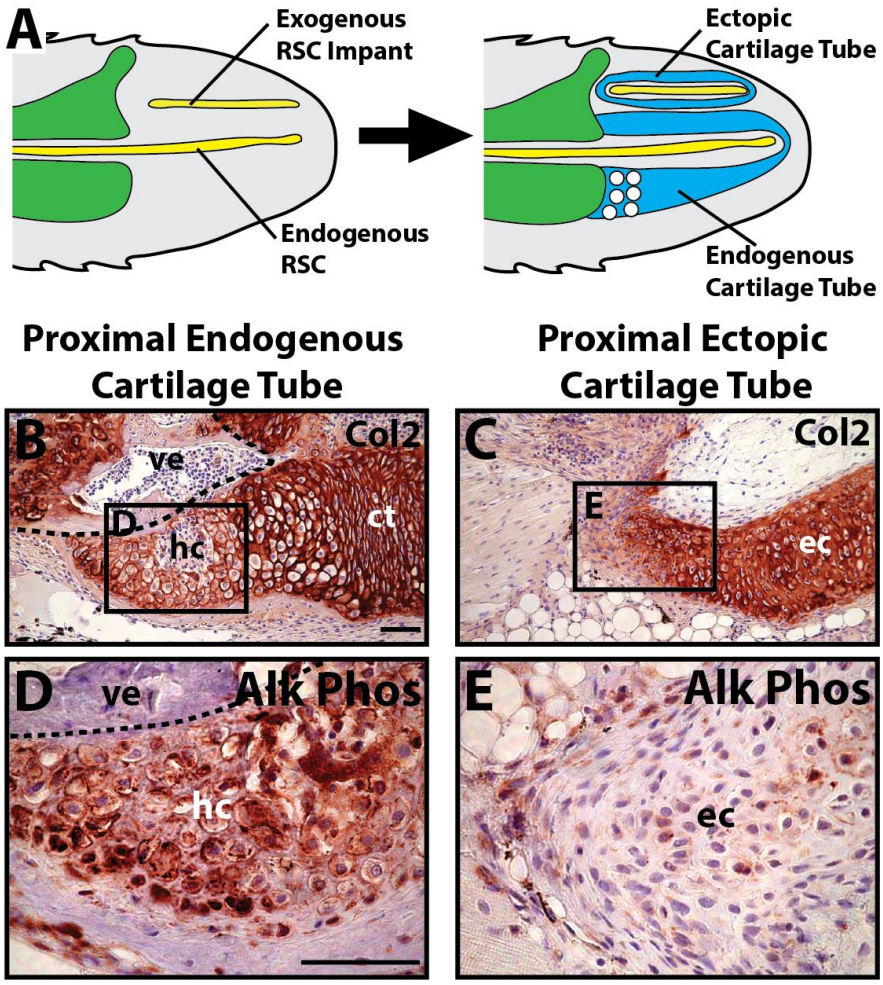

Fig. S8: Proximal lizard cartilage hypertrophy is dependent on the original tail vertebra. (A) Endogenous regenerated spinal cords and exogenous spinal cord implants induce formation of endogenous and ectopic CTs, respectively. However, ectopic and endogenous cartilage differed at their proximal ends, because only proximal endogenous cartilage makes contact with original tail vertebrae. Proximal **(B)** endogenous and **(C)** ectopic cartilage analyzed by Col2 immunostaining. **(D,E)** Higher magnification views of proximal cartilage regions identified in Panels B and C analyzed by Alk Phos immunostaining. Alk Phos+ hypertrophic chondrocytes were only detected in proximal endogenous cartilage areas, which contact the original tail vertebrae. Thus, these results suggested that proximal cartilage hypertrophy is linked to original tail vertebrae. Vertebrae boundaries are traced in dashed lines. ct, cartilage tube; ec, ectopic cartilage tube; hc, hypertrophic chondrocytes; ve, vertebra. Bar = 100 μm.

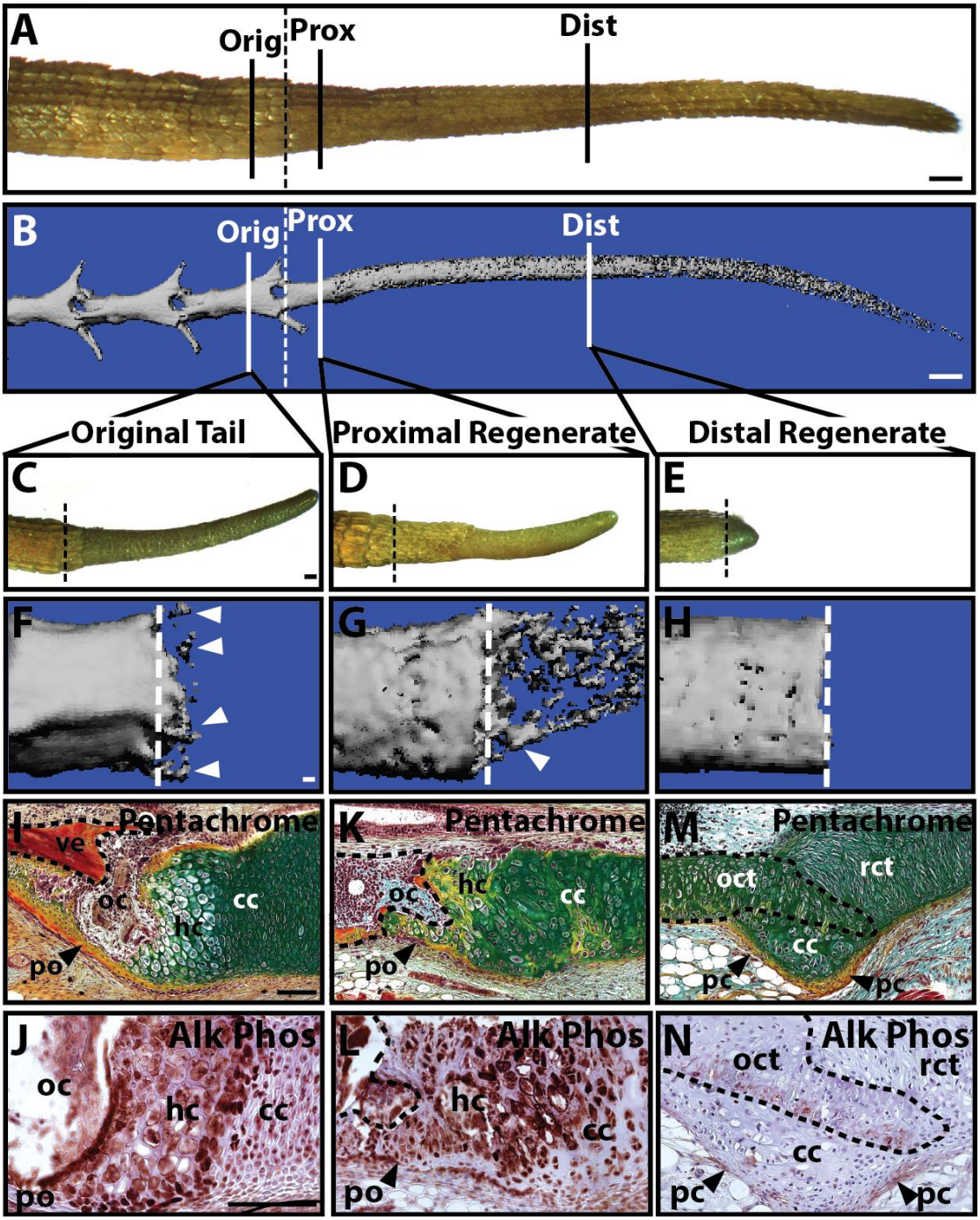

Fig. S9: Lizard tails amputated in osseous, but not cartilaginous, regions, regenerate cartilage that undergoes hypertrophy and endochondral ossification. Results in presented in Figure S6 suggested that proximal cartilage hypertrophy is induced by terminal tail vertebrae. However, what if lizard tails were re-amputated in the regenerated portion? Would the tails "re-regenerate"? If so, would new proximal cartilage regions undergo hypertrophy and ossify without physical interaction with original tail vertebrae? Here we considered these questions and tested whether pro-hypertrophy signals are specific for original tail vertebrae, or if proximal cartilage undergoes hypertrophy and endochondral ossification regardless of the skeletal tissue type present at the amputation site. **(A,B)** Mature lizard tail regenerates with CTs were amputated in (1) the original tail vertebra (Orig), (2) the ossified proximal regenerated tail (Prox), or (3) the partially calcified cartilaginous distal regenerated tail (Dist). In this way, the effects of three different

skeletal tissues (original tail bone, regenerated bone, and CT) on cartilage hypertrophy, endochondral ossification, and overall regeneration were studied. **(A)** Morphological and **(B)** microCT analyses of an intact mature lizard regenerate showing relative position of amputation sites. Following 4 weeks of regeneration, tails amputated in the **(C,F,I,J)** original tail, **(D,G,K,L)** proximal regenerate, or **(E,H,M,N)** distal regenerates were analyzed for **(C-E)** overall regenerate elongation and **(D,H,L)** amputation site ossification. Amputations to **(C)** original (30/n=30) and **(D)** regenerated bone (10/n=10) resulted in sizeable regenerates, while amputations to **(E)** CTs yielded only minimal, stunted regeneration (9/n=10). CTs regenerated from **(F)** original (30/n=10) or **(G)** regenerated osseous regions (10/n=10) exhibited ossification at amputation sites, while **(H)** CTs regenerated from cartilaginous regions did not exhibit any mineralization (10/n=10). **(I-N)** Higher magnification views of amputation sites analyzed by **(I-M)** pentachrome histological staining and (J-N) Alk Phos IHC. **(I,J)** Skeletons regenerated following original tail amputations developed proximal regions that bore striking similarities to CCs formed during fracture healing in higher vertebrates (30/n=30). Here, each CC involved an ossification center bordered by callus borders continuous with the periosteum of the original tail vertebrae and the perichondrium of regenerated skeleton. **(J)** Proximal CCs also developed growth plate-like zones with an abundance of Alk Phos^{+} hypertrophic chondrocyte. **(K,L)** Amputations in ossified proximal regenerated tails also resulted in CCs that ossified and joined the periosteum and perichondrium of osseous and cartilaginous skeletons, respectively (10/n=10). Compared to CCs observed in tails regenerated from amputations to original tail vertebrae, CCs formed from amputations to proximal regenerates exhibited disorganized proximal growth-plate like structures with **(L)** similarly disorganized regions of Alk Phos expression. **(M-N)** Finally, cuts to distal regenerated cartilaginous regions formed CCs that did not develop ossification centers (10/n=10). These CCs were bordered by perichondrium that linked original and regenerated cartilage. Regenerated cartilage did not exhibit growth-plate like zones or hypertrophic chondrocytes and **(N)** did not express Alk Phos (Alk Phos expression was limited to the perichondrium of "old", amputated CTs). In summary, both osseous and cartilaginous skeletons formed CCs in response to amputation, but only CCs developed from osseous tissues developed through hypertrophy and ossification. cc, cartilage callus; hc, hypertrophic chondrocytes; oc, ossification center; oct, original cartilage tube; pc, perichondrium; po, periosteum, rct, regenerated cartilage tube. (A-D) Bar = 0.5 cm, (F-N) Bar = 100 μm.

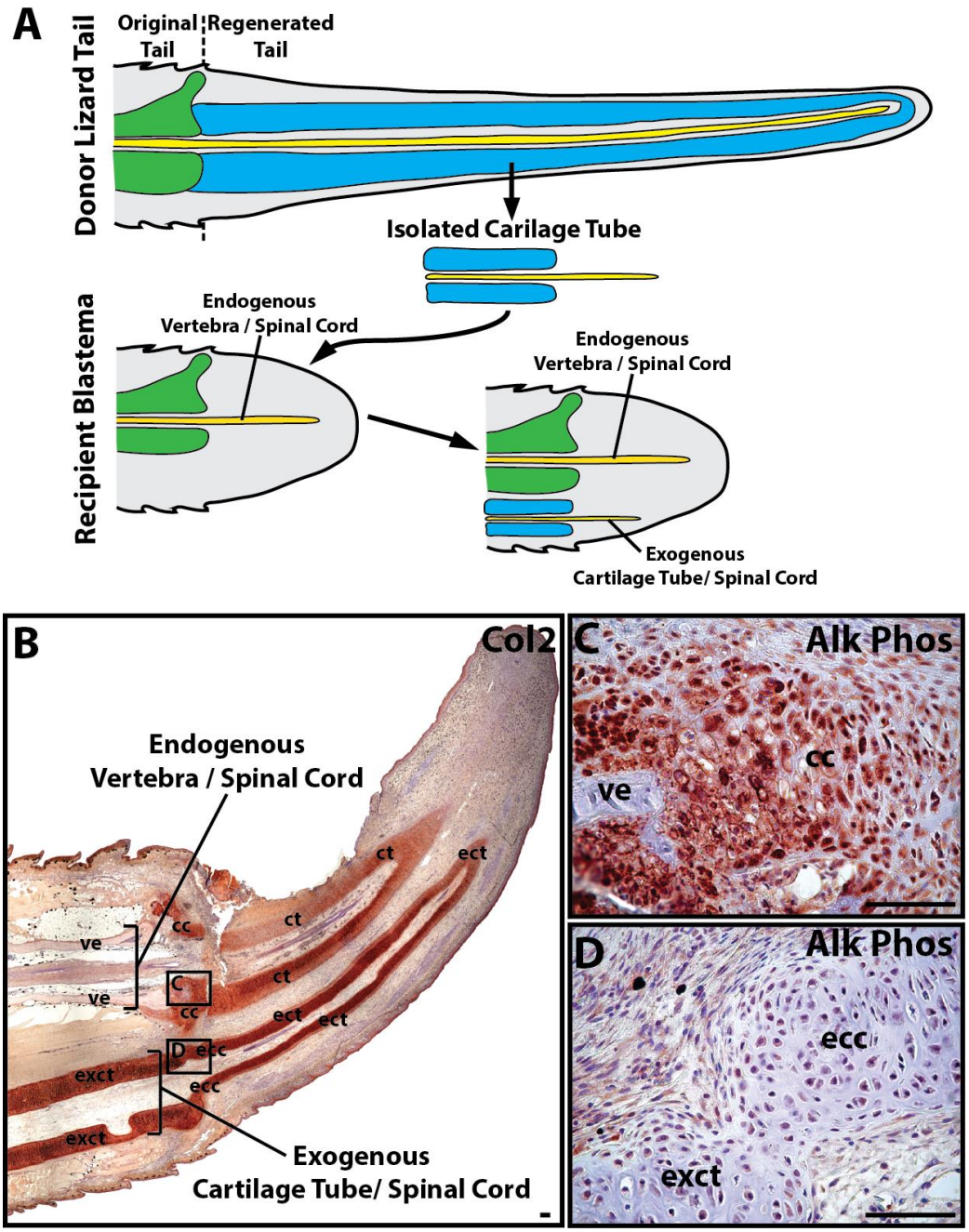

Fig. S10: Proximal cartilage hypertrophy is independent of the proximal lizard tail environment and dependent on original tail vertebrae. The following set of experiments controlled for the distal versus proximal regenerated tail environments and their effects on cartilage development. Our previous studies identified the original tail vertebrae as the candidate source of signals responsible for inducing cartilage hypertrophy and endochondral ossification. But we had not ruled out the original tail muscle, musculature, etc. as possible contributors of pro-hypertrophy signals. Previous studies done in the 1960's demonstrated that CTs with intact spinal cords induced formation of new CTs when implanted into original tail stumps (Simpson, 1964). Here, we sought to repeat these studies with the intention of examining the proximal cartilage areas induced by distal cartilage tube/spinal cord implants. **(A)** CTs with intact spinal cords were isolated from distal regions of donor regenerated tails and implanted into recipient original tail blastemas with endogenous vertebra and spinal cords (see Figure S5 for specifics of surgical manipulations). **(B)** Blastemas 2 weeks following implantation of

exogenous cartilage tube/spinal cord analyzed by Col2 IHC. Endogenous vertebrae and exogenous CTs induced formation of endogenous and ectopic CCs/CTs (4/n=6). Both endogenous and ectopic cartilage contacted skeletal elements within the proximal tail environment. Endogenous proximal cartilage contacted endogenous vertebrae, while ectopic proximal cartilage contacted CT implants. **(C, D)** Higher magnification views of proximal **(C)** endogenous CC and **(D)** ectopic CC regions identified in Panel B analyzed with Alk Phos immunostaining. Cartilage in contact with endogenous vertebrae exhibited hypertrophic morphologies and Alk Phos staining (4/n=4), while ectopic cartilage in contact with CT implants did not develop hypertrophy regions and did not express Alk Phos (4/n=4). These results suggested that vertebrae-derived signals, and not signals derived from other stump/proximal regenerated tail tissues, induce cartilage hypertrophy.

cc, endogenous cartilage callus; ct, endogenous cartilage tube; ecc, ectopic cartilage callus; ect, ectopic cartilage tube; exct, exogenous cartilage tube implant; ve, vertebrae. Bar = 100 μm.

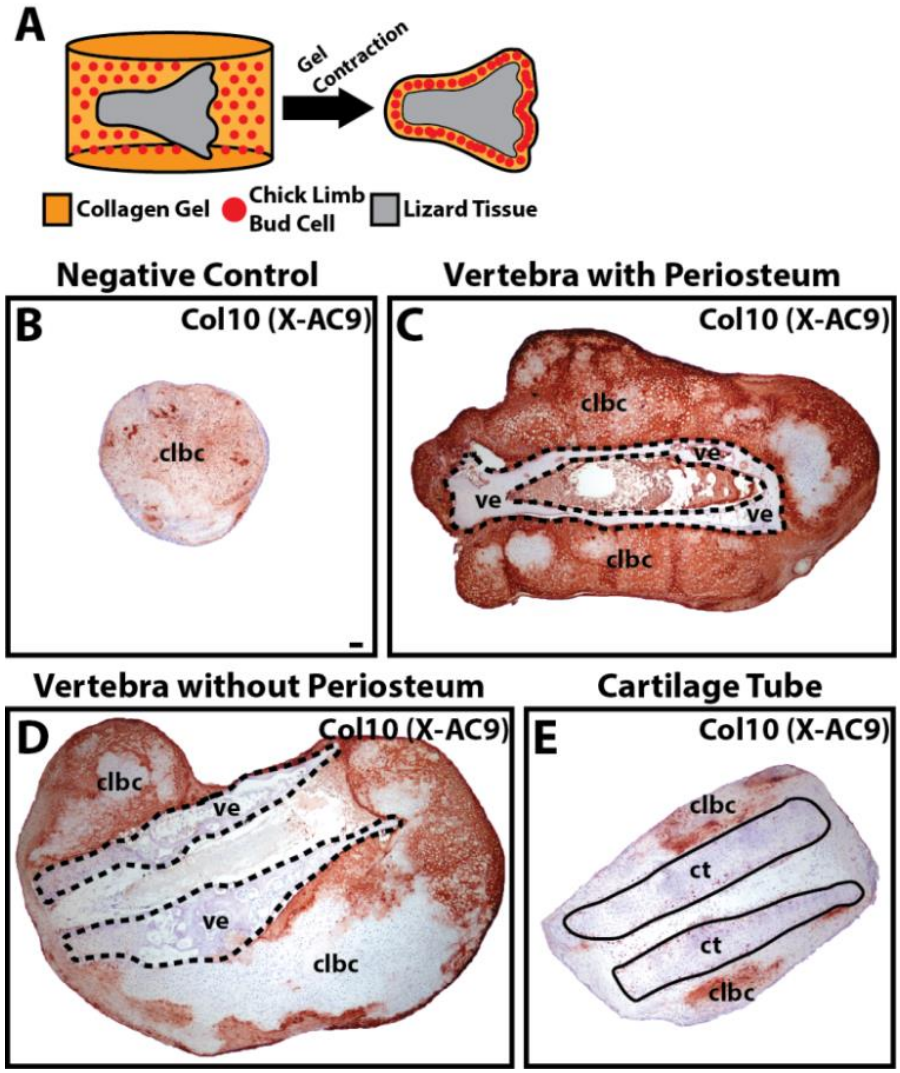

Fig. S11: Lizard vertebrae, but not CTs, induce hypertrophy in chick limb bud mesenchyme. Thus far, results suggested that signals derived from the vertebrae and periosteum induce periosteum-derived cartilage to undergo hypertrophy. However, additional work was needed to elucidate the dependence of proximal cartilage hypertrophy on vertebrae/periosteum signals rather than cells. Addressing this topic posed several technical challenges stemming from difficulties associated with distinguishing between signals and cells derived from the same tissues. To perform these experiments, we took advantage of xenogeneic co-cultures between lizard skeletal tissues and chick limb bud cells. Unlike salamander tissues, lizard tissues survive at the sample temperatures and medium osmolarities as chick and mammalian cells, thereby allowing for co-cultures between lizard tissues and these other cell types. Chick limb bud cells have been extensively used in in vitro models of cartilage development due to the abilities of embryonic limb bud mesenchyme to develop cartilage that undergoes hypertrophy and terminal differentiation under culture (Mello and Tuan, 1999). Adding to the attractiveness of this model is the availability of well-validated, species-specific antibodies to the established cartilage hypertrophy marker Col10. The X-AC9 clone mouse monoclonal antibody recognizes chicken, but not lizard, Col10 (Fig. S7) (Lozito and Tuan, 2015). Thus, xenogeneic lizard-chick co-cultures were used to specifically study the effects of lizard vertebra and periosteum on hypertrophy markers in cartilage formed from chick cells by eliminating contributions from lizard hypertrophic cartilage.

(A) We developed a system for co-culturing chick cells with lizard skeletal tissues in 3-dimensional constructs. Chick cells were suspended in Col1 gels, which were cast over lizard skeletal tissues. Enzymatic and mechanical activities of chick cells caused gels to contract around the lizard tissues within 5 days, allowing for both direct and indirect interactions between lizard tissues and chick cells **(B-E)** After 3 weeks of growth, xenogeneic co-cultures were immunostained for Col10 (X-AC9) to identify chick hypertrophic cartilage regions. **(B)** Negative control samples consisted of chick limb bud cells only, without lizard tissues. Experimental samples involved co-culturing chick cells and **(C)** lizard vertebrae with intact periosteum, **(D)** lizard vertebrae lacking periosteum. **(E)** Co-cultures between lizard distal CTs and chick limb bud cells were included as tissue-type controls. (As presented above, distal CT tissue did not induce hypertrophy in lizard cartilage, and we wanted to validate the relevancy of xenogeneic cultures by testing the effects of lizard CTs on chick cartilage.) In conditions involving lizard vertebrae and CTs, samples included the same amount of lizard tissues (5 mg wet weight). **(C)** Lizard vertebrae induced significant increases in overall cartilage formation and Col10 expression (6/n=6) compared to **(B)** negative and **(E)** lizard CT tissue-type controls. **(D)** Removal of periosteum prior to co-culture did not affect vertebra-induced increases in overall cartilage formation but did significantly decrease Col10 expression (6/n=6) compared to **(C)** vertebra samples with intact periosteum, but not to basal levels seen in **(B)** negative and **(D)** tissue-type control samples. These results confirmed lizard original tail vertebra and periosteum as the sources of pro-cartilage hypertrophy signals.

Dashed lines mark vertebra tissue boundaries, and solid lines trace CT tissue boundaries. clbc, chick limb bud cells, ct, lizard ct, ve, lizard vertebra. Bar = 100 μm.

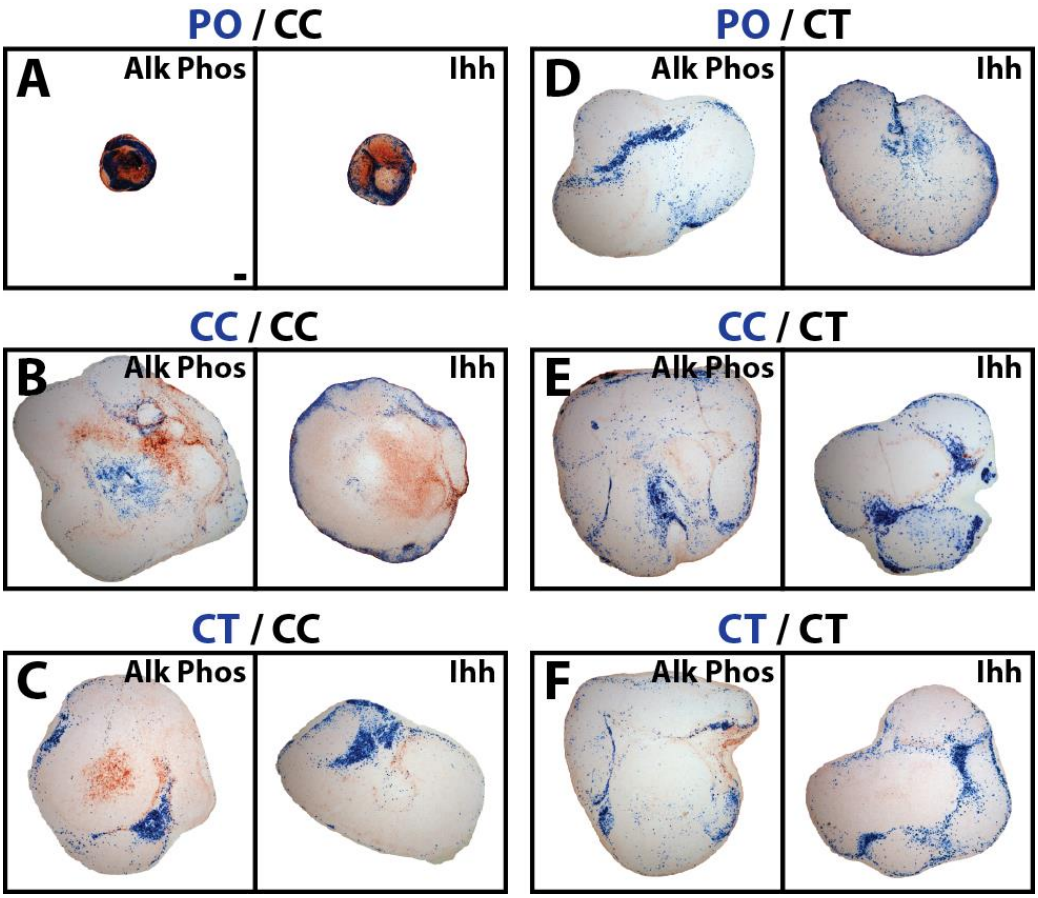

Fig. S12: Lizard periosteal cells induce hypertrophy and Ihh expression in CC, but not CT, cells. (A-F) Lizard periosteal (PO), cartilage callus (CC), and cartilage tube (CT) cells isolated and labeled with CFDA-SE (designated by blue text color in sample titles) and mixed 1:20 with unlabeled CC or CT cells (designated by black text color in sample titles) and pellet cultured for 3 weeks. Samples were co-immunostained for FITC, which stains blue, and either Alk Phos or Ihh, which stains red. **(A)** PO / CC co-cultures were significantly smaller and exhibited higher expression of Alk Phos and Ihh compared to **(B)** CC / CC or **(C)** CT / CC co-cultures. **(D)** PO cells did not affect CT culture size or induce CT Alk Phos or Ihh expression, and, overall, **(E, F)** CT cells exhibited minimal Alk Phos expression. Bar = 100 μm.

These results suggest that vertebral periosteal cells induce hypertrophy and Ihh expression in CC, but not CT, cells. These results also confirm the observations that CC, but not CT, cells respond to periosteal cell-derived signals by undergoing hypertrophy.

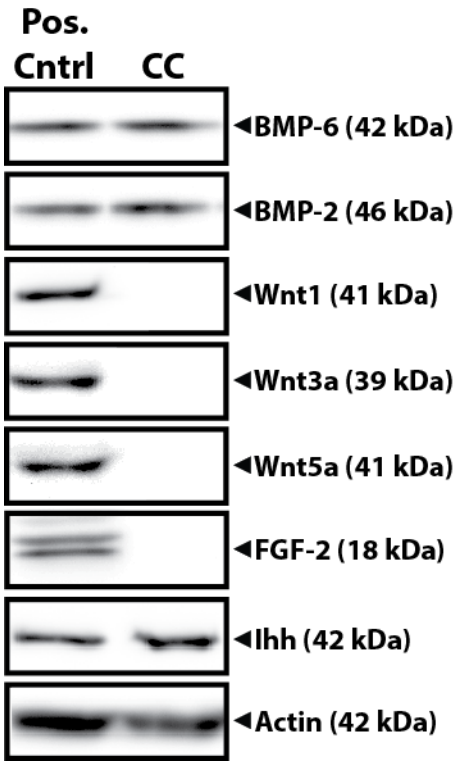

Fig. S13: Analysis of growth factors present in lizard tail CC. CC protein was isolated from lizard tails 14 DPA and analyzed by BMP-6, BMP-2, Wnt1, Wnt3a, Wnt5a, FGF-2, and Ihh Western blots. Protein samples isolated from embryonic lizard limb buds were included as positive controls.

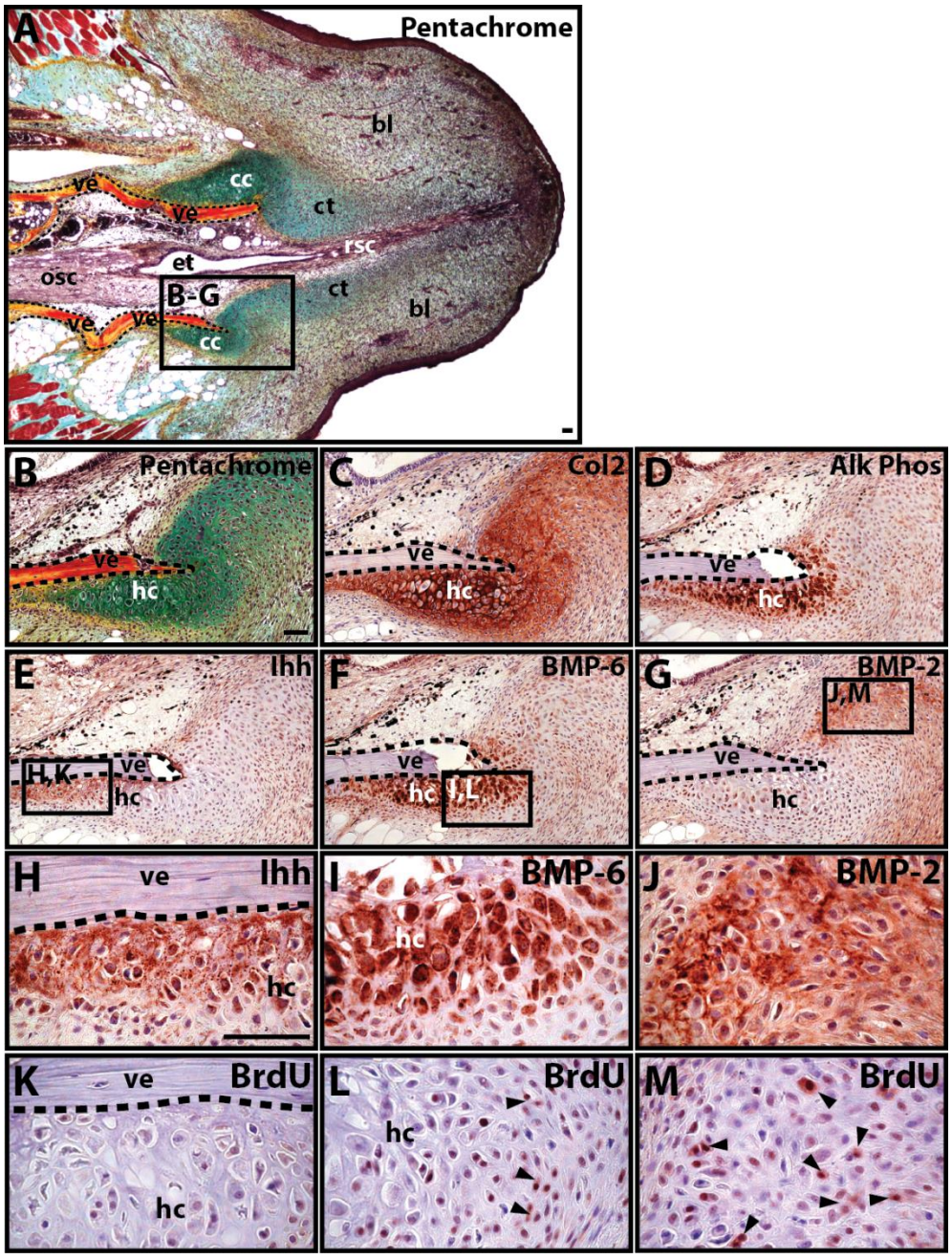

Fig. S14: Proximal cartilage hypertrophy and proliferation localize with Ihh and BMP expression, respectively. In order to study the mechanisms regulating proximal cartilage development, we began by characterizing expression of signaling molecules within the developing proximal cartilage environment. **(A)** Early regenerates (14 DPA) analyzed by pentachrome staining showed initial development of proximal CCs. **(B-I)** Higher magnification views of regions identified in Panel A analyzed by **(B)** histology (pentachrome) or **(C)** Col2, **(D)** Alk Phos, **(E)** Ihh, **(F)** BMP-6, and **(G)** BMP-2 immunostaining. **(H-M)** Higher magnification views of regions identified in Panels E-G. **(K-M)** BrdU immunostaining was used to identify proliferative cells, some of which are identified by black arrow heads. Dashed lines mark vertebral boundaries. bl, blastema; cc, cartilage tube; ct, cartilage tube; et, ependymal tube; hc, hypertrophic chondrocytes; osc, original spinal cord; rsc, regenerated spinal cord; ve, vertebra. Bar = 50 μm

(A) In early regenerates, the majority of the blastemas remained undifferentiated, as evidenced by sparse muscle formation and incomplete glycosaminoglycan deposition by developing CTs. The exception were proximal CCs, which

already exhibited characteristic cartilaginous matrix rich in **(A,B)** glycosaminoglycans and **(C)** Col2. That proximal CCs develop before CTs form from blastemal cells is another clue to their independent formation. **(D)** Proximal CCs contacted terminal tail vertebrae, and these contact regions underwent hypertrophy and expressed Alk Phos. **(E)** Ihh localized to anterior CCs and was highly associated with vertebrae **(H)**, being expressed by both the bone tissue adjacent cartilage regions. **(F)** BMP-6 expression localized to medial CCs and was expressed by hypertrophic chondrocytes **(I)**. **(G)** BMP-2 was expressed by the anterior CC and at the junction between CCs and CTs **(J)**. **(K-M)** BrdU immunostaining was used to identify proliferative cartilage regions. **(K)** Very few proliferative cells were detected in posterior CCs near original tail vertebrae, and the vast majority of proliferative cells were detected in **(L)** medial and **(M)** posterior zones, both of which overlapped with BMP staining **(I,J)**. Thus, these results demonstrated anterior, medial, and posterior localizations of Ihh, BMP-6, and BMP-2 expression, respectively, within regenerated lizard tail CCs. Such findings also linked these signaling molecules with processes of proximal CC development: induction, proliferation, and hypertrophy. Ihh was associated with the vertebrae, which we showed above was involved in proximal CC induction. Proximal cartilage tube proliferation co-localized with BMP-2 and BMP-6 expression, and cartilage hypertrophy overlapped with both Ihh and BMP regions.

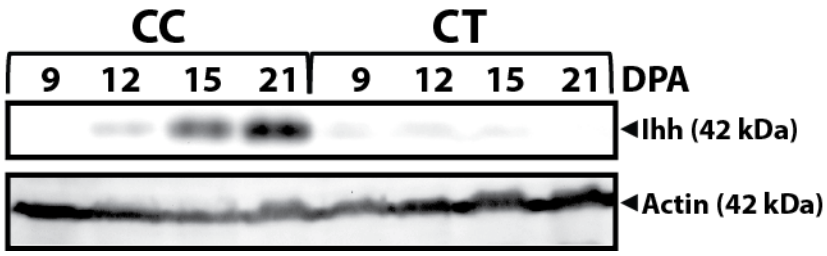

Fig. S15: Time course of CC and CT Ihh expression during early lizard tail regeneration. Protein collected from proximal CC and distal CT regions 9-21 DPA were analyzed by Ihh Western blots.

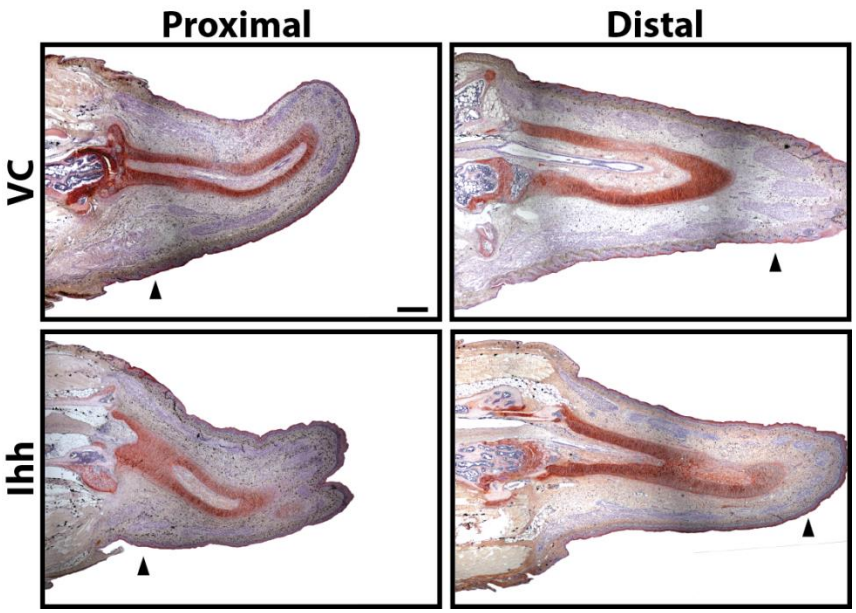

Fig. S16: Ihh-beads do not affect either proximal or distal cartilage formation. Beads soaked in 1mg/ml Ihh or vehicle control (VC) were implanted in the ventral surfaces of either proximal or distal regions of 9 DPA blastemas (implantation sites marked by arrow heads). After two weeks of explant culture, samples were immunostained for Col2. Treatment with Ihh-beads did not significantly affect cartilage formation. Bar = 500 µm.

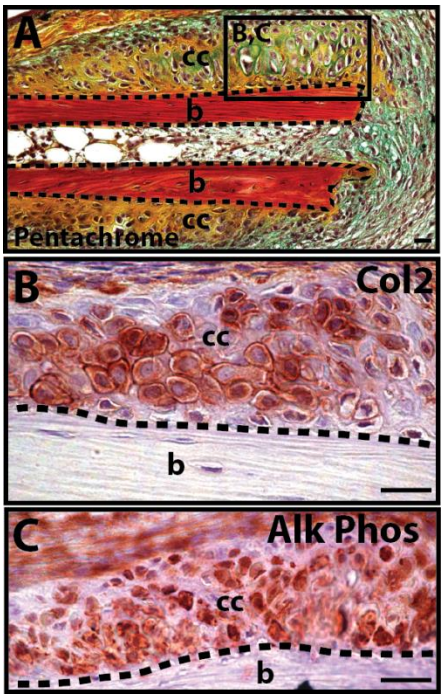

Fig. S17: Cartilage regeneration independent of blastema. (A) Lizard toe 14 days after amputation analyzed by histology (pentachrome). **(B, C)** Higher magnification views of regions identified in Panel A analyzed by **(B)** Col2 and **(C)** Alk Phos immunostaining. Dashed lines mark bone boundaries. b, bone; cc, cartilage callus. Bar = 50 µm.

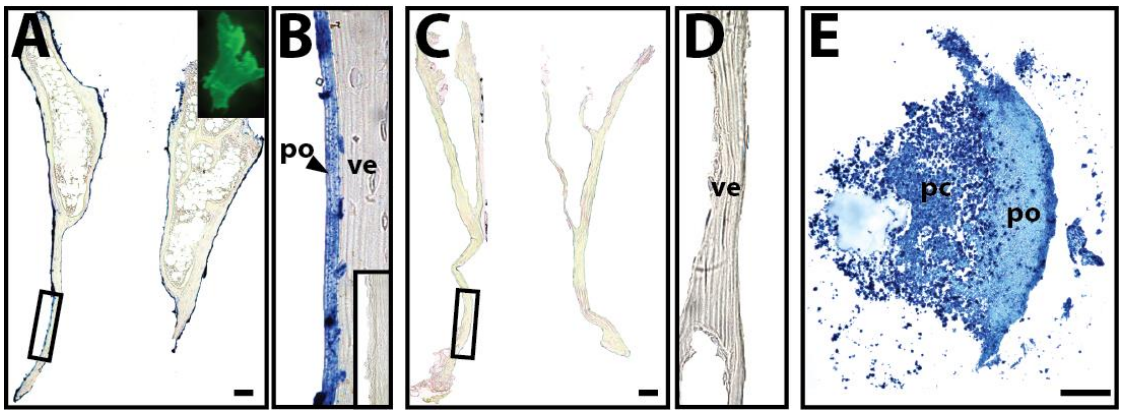

Fig. S18: Selective labeling and isolation of lizard tail vertebra periosteum. **(A)** Sagittal section of a lizard tail vertebra treated with CFDA-SE and analyzed by FITC immunostaining. (Here, distal is directed upwards.) FITC-labeled cells and tissues appear blue. **(A, Inset)** Fluorescence micrograph of CFDA-treated vertebra. **(B)** Higher magnification view of region identified in Panel A highlighting specific FITC labeling of the periosteum. **(B, Inset)** Periosteum of control, unlabeled vertebra. **(C)** Periosteum was removed from CFDA-SE-treated vertebrae, and the remaining tissue was analyzed by FITC immunostaining. **(D)** Higher magnification view of region identified in Panel D demonstrating effective removal of periosteum. **(E)** To validate periosteal cell isolation, periosteal tissue removed from CFDA-SE-treated vertebrae were cultured as explants according to Supplementary Methods for 1 week and analyzed by FITC immunostaining. Cell populations that crawled out of labeled periosteal tissue contained high levels of FITC, indicating enrichment of periosteal cells. pc, periosteal cells; po, periosteum; ve, vertebra. A-E: Bar = 250 μm; F: Bar = 50.

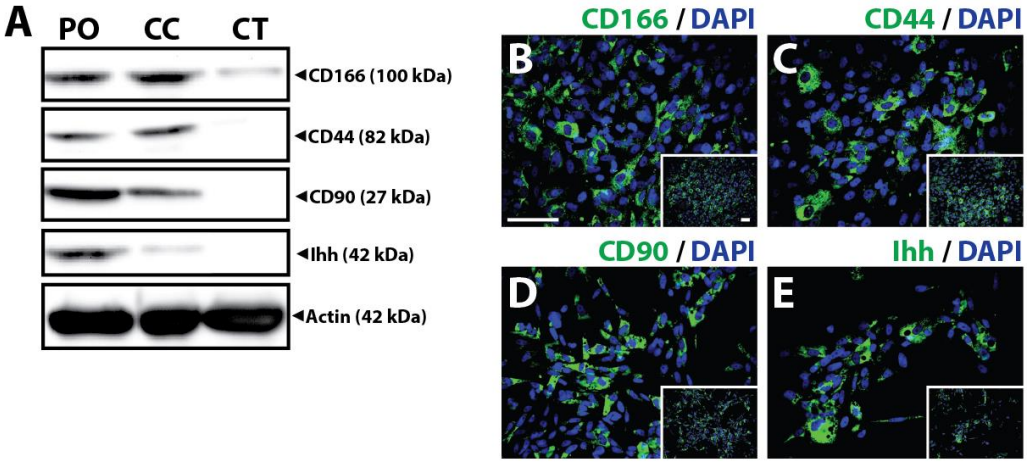

Fig. S19: Lizard periosteal and CC cells express the stem/progenitor cell markers CD166, CD44, and CD90. (A) Cultured cells isolated from lizard periosteal (PO), cartilage callus (CC) and cartilage tube (CT) cells were analyzed by Western blot for expression of the periosteal stem/progenitor cell markers CD166, CD44, and CD90 and for Ihh expression. PO and CC, but not CT, cells expressed high levels of CD166, CD44, and CD90. Only PO cells secreted Ihh in culture. **(B-E)** Periosteal cell expression of CD166, CD44, CD90, and Ihh was validated with immunofluorescence. Bar = 25 μm.

These results identify $CD166^{+}$ $CD44^{+}$ $CD90^{+}$ periosteal stem/progenitor cells as the vertebral source of Ihh, the signal responsible for inducing Alk Phos expression in lizard CC cells. Furthermore, the fact that periosteal markers are also detected in the lizard tail CC further supports the hypothesis that the CC is derived from periosteal cells.

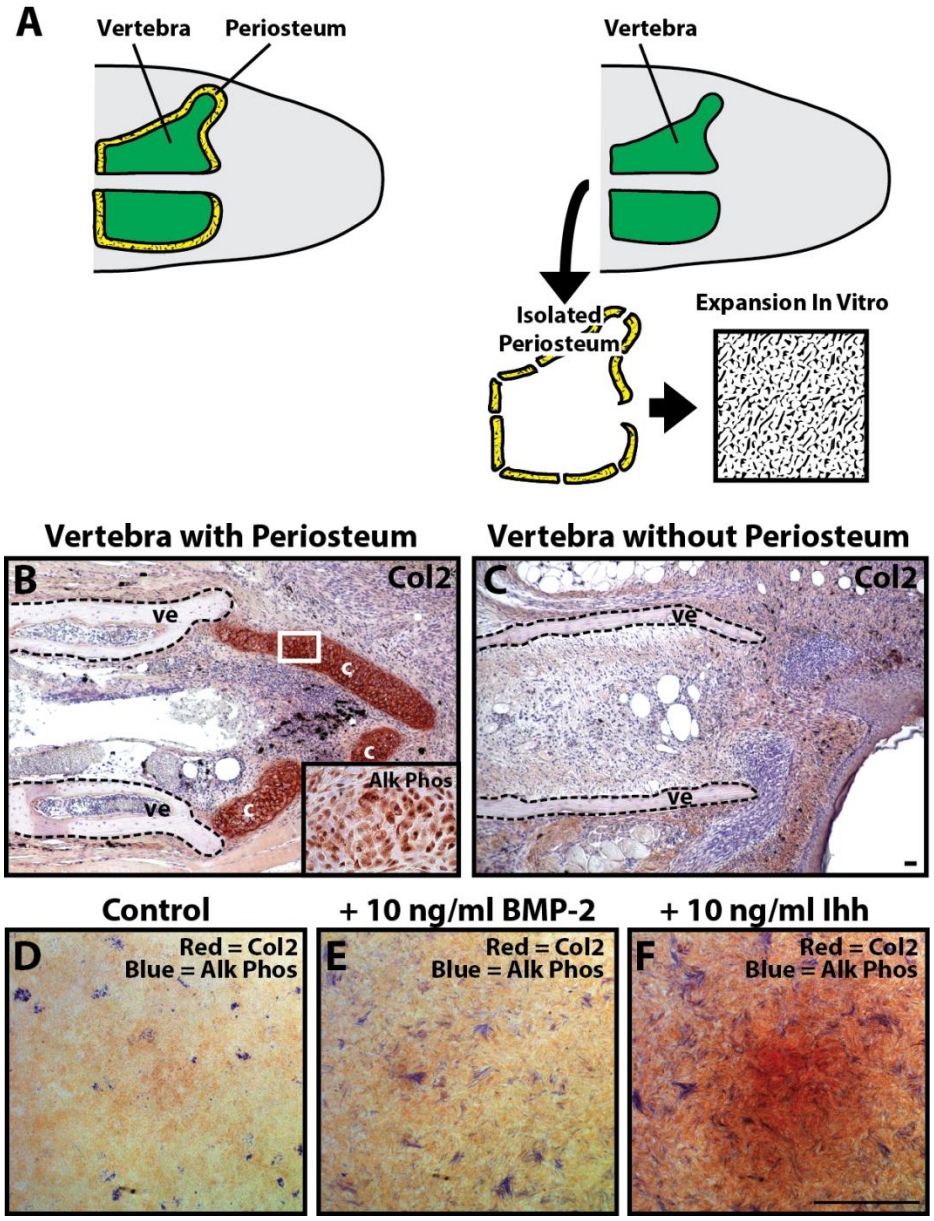

Fig. S20: The proximal regenerated lizard tail skeleton is derived from the periosteum of original tail vertebrae. As presented in Figure S13, the labeling scheme employed in fate-mapping studies preferentially labeled the periosteum of vertebrae (Fig. S13A,B), suggesting that the periosteum is the specific tissue source of the proximal CC. Indeed, the mammalian periosteum is known to harbor populations of stem cells that form CCs during fracture repair (Colnot, 2009). Here we sought to study this directly by testing whether removal of periosteum affected the ability of lizard vertebrae to form cartilage. Periosteum removal was validated, (Fig. S13C,D), and isolated periosteal cells (Fig. S13E) were collected and cultured for experimentation, as described below.

(A) Experimental setup used to investigate role of periosteum in proximal cartilage development. Tails containing vertebrae with intact periosteum and tails containing vertebrae treated to remove periosteum were compared for cartilage formation. Isolated periosteum was used to generate periosteal cells that were expanded in vitro. Spinal cords were also removed from vertebrae/blastemas to focus on vertebra-derived cartilage. **(B)** Vertebrae with intact periosteum formed cartilage (3/n=3) that expressed (3/n=3) Alk Phos **(B, Inset)**, while **(C)** vertebrae without periosteum did not form

cartilage (7/n=7). These results indicated periosteal cells as the source of Alk Phos-expressing cartilage. **(D-F)** For further validation, we performed studies on cells isolated from collected periosteum and tested their responses to hedgehog and BMP signals. Periosteal cell micromass cultures were stained for Alk Phos (Blue) and immunostained for Col2 (Red). **(D)** Populations of perichondral cells cultured under control conditions expressed Alk Phos (3/n=3), while Col2 was undetectable (0/n=3). **(E)** Treatment with 10 ng/ml BMP-2 induced proliferation of Alk Phos-positive cell populations (3/n=3), but Col2 remained undetectable (0/n=3). **(F)** Treatment with 10 ng/ml Ihh stimulated Alk Phos expression and Col2 production. Combined with results from drug/growth factor experiments involving lizard tail blastema explants described in the main article (Fig. 4-6), these results suggested that Alk Phos-positive cartilage of the proximal CC is derived from the perichondrium of vertebrae, and that periosteum-derived cells respond similarly to BMP and hedgehog signaling compared to proximal cartilage.

Dashed lines mark vertebral boundaries. c, cartilage; ve, vertebrae. Bar = 100 μm.

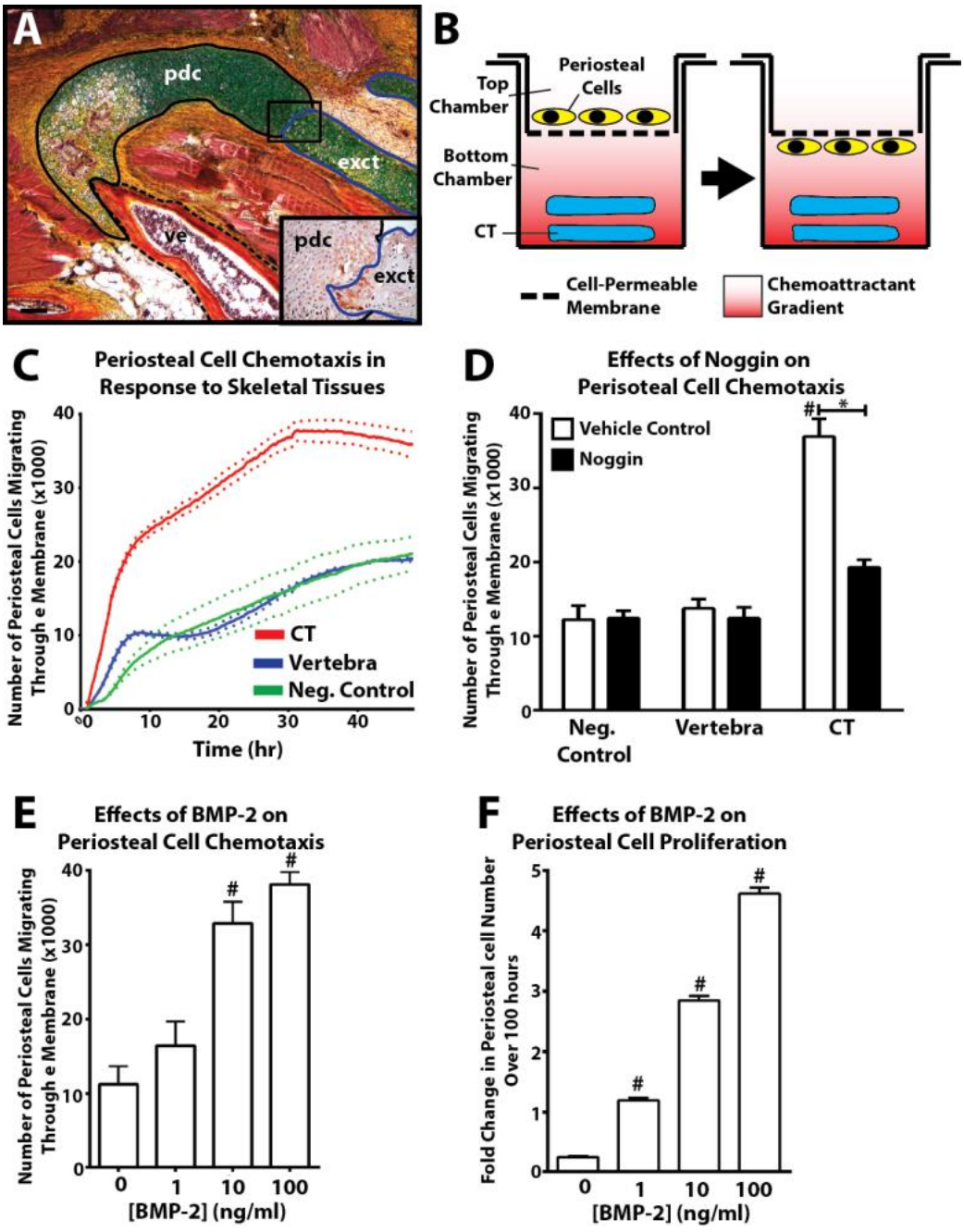

Fig. S21: Lizard CTs induce migration and proliferation in periosteal-derived cells and cartilage via BMP-2. This group of studies considered crosstalk between CC and CT areas and its effect on skeletal regeneration. **(A)** During CT transplantation studies, we observed dramatic expansion and migration/invasion of periosteal-derived cartilage in response to CT implants. Periosteal-derived cartilage was observed bridging gaps between CT implants and vertebrae as they migrated (5/n=5), even creating dramatic bends. Panel A presents histological (pentachrome) analyses of an example of directed CC growth between original tail vertebrae and exogenous CT implants (EXCT), and **(A, Inset)** a higher magnification view of the CC/EXCT interface region immunostained for BMP-2. That CTs were able to induce proliferation and migration of periosteal cell-derived cartilage without direct physical contact suggested that soluble factors secreted by the CTs were involved, and we used migration assays to test the chemotactic effects of CT-derived soluble factors on periosteal cell migration. **(B)** Schematic representing migration assays used to measure effects of lizard

tail tissue on periosteal cell chemotaxis. Migration assays included top and bottom chambers separated by cell-permeable membranes. Chemotaxis was measured as periosteal cell migration from top chambers toward bottom chambers containing CTs. Bottom chambers containing original tail vertebrae were included as tissue-type controls, and empty bottom wells were included as negative controls. In conditions involving lizard CTs and vertebrae, bottom chambers included the same amount of lizard tissues (5 mg wet weight). **(C)** Representative real-time migration assay plot of lizard periosteal cell chemotaxis towards lizard CT or vertebra tissue or vehicle control over 24 hours. Lizard CTs caused significant migration of lizard periosteal cells compared to both negative and tissue-type controls (n=3). These results suggested that factors released by lizard CTs direct migration of periosteal-derived cells.

In order to determine the specific factors responsible for periosteal cell chemotaxis toward CT implants, we screened for signaling molecules expressed at the junction between periosteal-derived cartilage and CT implants. BMP-2 was detected along the interface between the two cartilage regions **(A, Inset)**, similar to the BMP-2 expression pattern observed at the junction between the proximal and CT regions (Fig. S11G). Thus, we hypothesized that BMP-2 was a candidate chemoattractant secreted by the CT that acts on periosteal-derived cartilage. First, the effects of the BMP antagonist noggin on CT-induced periosteal cell chemotaxis was investigated. **(D)** Migration assays were prepared as described above, but with lizard CTs and vertebrae added to bottom chambers in the presence of 100 ng/ml noggin or vehicle control (n=3). Noggin treatment significantly decreased periosteal cell chemotaxis compared to controls, suggesting that BMPs were at least partially responsible for migration induced by CT-secreted factors. **(E)** Finally, we tested the effects of exogenous BMP-2 on periosteal cell migration and proliferation in the absence of CT tissue. Migration assays were prepared with BMP-2 solutions (0-100 ng/ml) in bottom chambers and periosteal cells in top chambers (n=3). BMP-2 proved to be a powerful chemoattractant to periosteal cells, inducing migration in a dose-dependent manner over 24 hours. **(F)** BMP-2 (0-100 ng/ml) also significantly enhanced periosteal cell proliferation in a dose-dependent manner over 100 hours (n=3). Taken together, these results suggest that CT-secreted BMPs, including BMP-2, induce migration and direct expansion of periosteal-derived proximal CCs. This has implications in patterning the proximal regenerated tail CC, and may explain the seamless junction between CC/CT regions with minimal extraneous cartilage development.

Boundaries of original tail vertebra are traced in dashed lines, solid blue lines trace the borders of CT implant, and solid black lines mark the outlines of periosteum-derived cartilage that bridge the gap between vertebrae and CT implants. exct, exogenous cartilage tube implant; pdc, periosteum-derived cartilage; ve, vertebra. Bar = 100 μm. #, $p < 0.05$, compared to vehicle control; *, $p<0.05$, compared to samples indicated by bars.

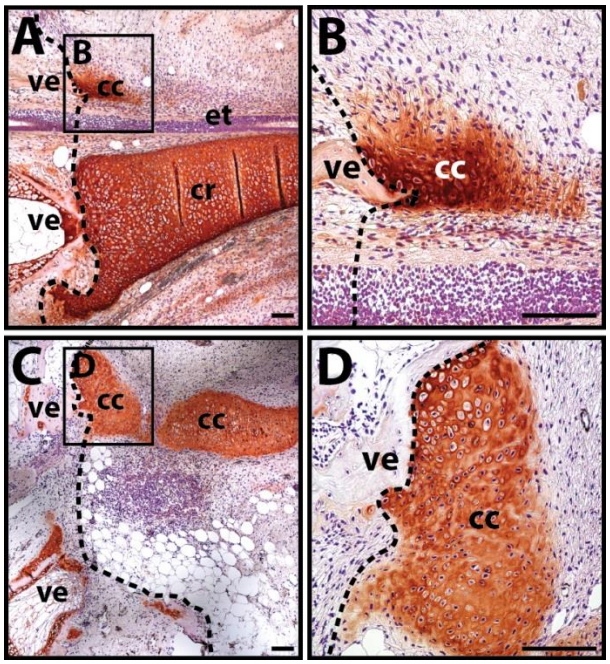

Fig. S22: Salamanders, like lizards, develop vertebra-derived CC regenerated tail regions. Regenerated salamander tails, with or without endogenous spinal cords, were studied for differences in cartilage development. **(A-D)** Sagittal section of proximal regions of regenerated salamander tail analyzed by Col2 immunostaining. **(A)** Control tails with spinal cords developed ventral CRs. Cartilage dorsal to the ependymal tube is only formed at the extreme proximal regenerated tail. **(B)** Magnified view of dorsal cartilage region identified in Panel A highlighting its association with the original tail vertebra. **(C)** Salamander tails without spinal cords did not develop CTs, but extensive cartilage formation was observed in dorsal regenerated tail regions. **(D)** Higher magnification view of dorsal cartilage regions identified in Panel C. Dashed lines denote boundaries between original (left) and regenerated (right) tail regions. cc, cartilage callus; cr, cartilage rod; et, ependymal tube; rsc regenerated spinal cord. Bar = 100 µm.ve, vertebra. Bar = 100 µm.

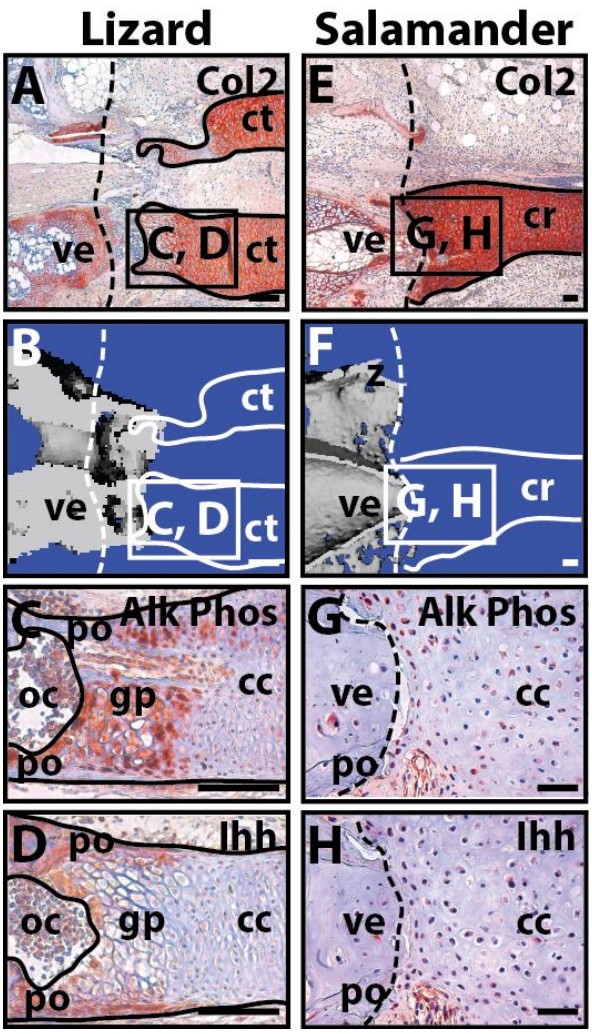

Fig. S23: Proximal lizard, but not salamander, cartilage undergoes endochondral ossification. (A-D) Lizard and (**E-H)** salamander proximal regenerated skeletons (sagittal sections) were analyzed by **(A, E)** Col 2 IHC, **(B, F)** microCT, and **(C, G)** Alk Phos and **(D, H)** Ihh IHC. Dashed lines denote boundaries between original (left) and regenerated (right) tail portions. Solid lines trace outlines of regenerated cartilage skeletons. cc, cartilage callus, cr, cartilage rod; ct, cartilage tube; gp, growth plate-like zone; ip; oc, ossification center; po, periosteum; ve, vertebra. Bar = 100 μm.

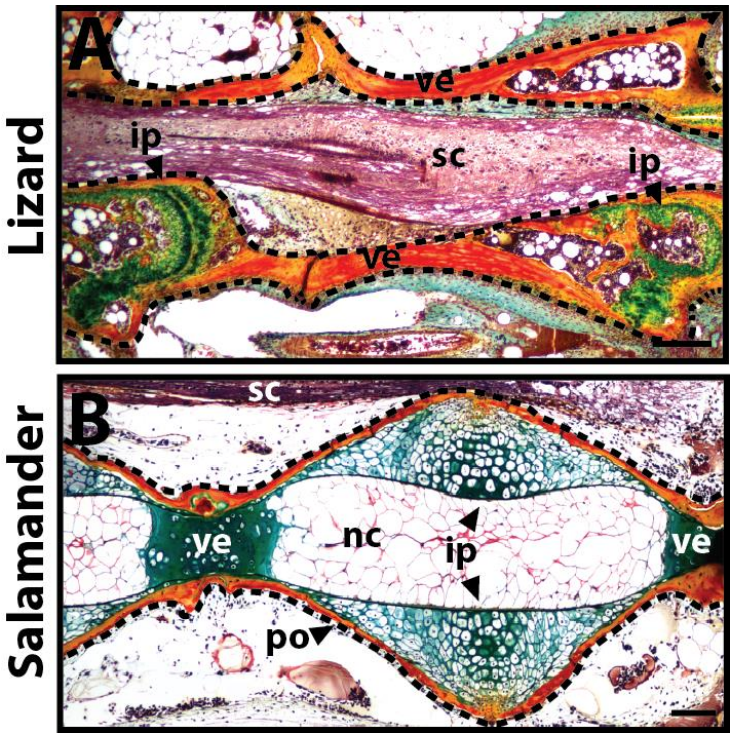

Fig. S24: **Adult lizard tail skeletons are ossified, while adult salamander tail skeletons are predominantly cartilaginous.** Original **(A)** lizard and **(B)** salamander tails analyzed by pentachrome histological staining. Ossified tissue stains red/orange, while cartilage stains green. The majority of lizard tail vertebrae ossify, and cartilage is restricted to unclosed growth plates and intervertebral pads. Salamander tail skeletons retain notochord tissue into adulthood, and the salamander centrum is predominantly cartilaginous (only the periosteum is ossified). Vertebral boundaries are traced in dashed lines. nc, notochord; ip, intervertebral pad; po, periosteum; sc, spinal cord; ve, vertebra. Bar = 100 μm.

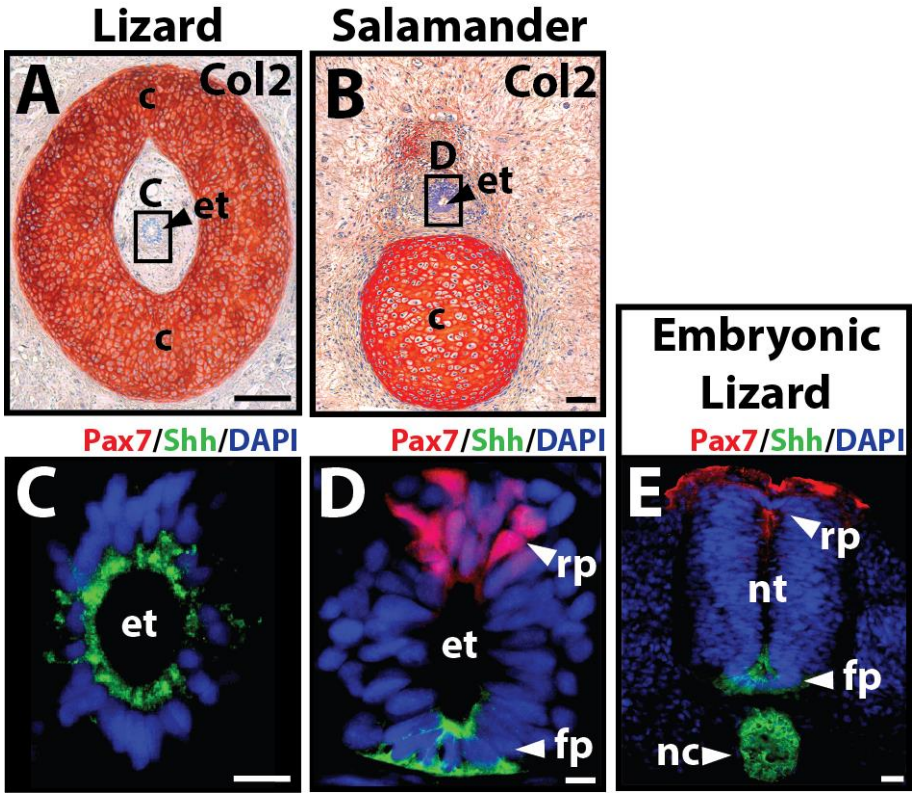

Fig. S25: Salamanders regenerate a cartilage rod, while lizards regenerate a cartilage tube. (A, B) Transverse sections of lizard and salamander regenerated skeletons analyzed by Col2 IHC. Bar = 100 µm. **(C)** Regenerated lizard tail ependymal tube, **(D)** regenerated salamander tail ependymal tube, and embryonic lizard neural tubes analyzed by Shh and BMP-2 IHC. Bar = 25 µm. cr, cartilage rod; ct, cartilage tube; et, ependymal tube; fp, floor plate; nc, notochord; nt, neural tube; rp, roof plate.

Table S1. IHC primary antibody information. Specific primary antibody product information is presented with antigen retrieval methods and antibody dilutions used. Where applicable, comments on antibody performance in IHC applications involving lizard and other animal tissues are also described. For enzymatic antigen retrieval, samples were incubated in 1 mg/ml chondroitinase and 5 mg/ml hyaluronidase for 30 min at 37°C, and for heat-mediated antigen retrieval, samples were treated with sodium citrate buffer, pH 6.0, for 20 min at 95°C followed by 20 min of cooling at room temperature. All primary antibody incubations were performed over 12-16 hours at 4°C. Similarly, all other methodology parameters (i.e., washing, blocking of endogenous peroxidase and nonspecific binding, incubations with secondary antibody and HRP-conjugated streptavidin, signal development, and imaging) were identical among primary antibodies used.

Target	Manufacturer (Product Code)	Antigen Retrieval Method	Antibody Dilution	Comments
Col2	Abcam (ab34712)	Enzymatic	1:400	Excellent reactivity with lizard and salamander tissues.
Shh	Novus Biologicals (NBP1-69270)	Heat-mediated	1:500	Excellent reactivity with lizard and salamander tissues.
Alk Phos	Abcam (ab108337)	Heat-mediated	1:250	Excellent reactivity with lizard and salamander tissues.
Ihh	Abcam (ab39634)	Heat-mediated	1:200	Excellent reactivity with lizard and salamander tissues.
BMP-6	Abcam (ab155963)	Heat-mediated	1:100	Expressed by hypertrophic lizard cartilage.
BMP-2	Abcam (ab14933)	Heat-mediated	1:200	Expressed by junction region at CC/CT interphase.
Col10 [X-AC9]	Abcam (ab140230)	Enzymatic	1:100	Very specific for chick Col10. Does not react with lizard or mammalian samples.
Col10	Abcam (ab58632)	Enzymatic	1:100	Detects Col10 in lizard and chick embryonic growth plate samples.
Pax7	Developmental Studies Hybridoma Bank (PAX7-c)	Heat-mediated	1:50	Excellent reactivity with lizard and salamander tissues.

SUPPLEMENTARY REFERENCES

Colnot, C. (2009). Skeletal Cell Fate Decisions Within Periosteum and Bone Marrow During Bone Regeneration**.** *Journal of Bone and Mineral Research*. **24**, 274-282.

DeLise, A. M., Stringa, E., Woodward, W. A., Mello, M. A., Tuan, R. S. (2000). Embryonic limb mesenchyme micromass culture as an in vitro model for chondrogenesis and cartilage maturation**.** *Methods in molecular biology*. **137**, 359-375.

Limame, R., Wouters, A., Pauwels, B., Fransen, E., Peeters, M., Lardon, F., De Wever, O., Pauwels, P. (2012). Comparative analysis of dynamic cell viability, migration and invasion assessments by novel real-time technology and classic endpoint assays**.** *PloS one*. **7**, e46536.

Lozito, T. P., Tuan, R. S. (2014). Endothelial and cancer cells interact with mesenchymal stem cells via both microparticles and secreted factors**.** *Journal of cellular and molecular medicine*. **18**, 2372-2384.

Mello, M. A., Tuan, R. S. (1999). High density micromass cultures of embryonic limb bud mesenchymal cells: an in vitro model of endochondral skeletal development**.** *In Vitro Cell Dev Biol Anim*. **35**, 262-269.

Sinha, R. K., Morris, F., Shah, S. A., Tuan, R. S. (1994). Surface composition of orthopaedic implant metals regulates cell attachment, spreading, and cytoskeletal organization of primary human osteoblasts in vitro**.** *Clin Orthop Relat Res*. 258-272.